ELSEVIER

Surface Science 337 (1995) 232–242

surface science

# LEED structure determination of hexagonal $\alpha$-SiC surfaces

J. Schardt, Ch. Bram, S. Müller, U. Starke *, K. Heinz, K. Müller

*Lehrstuhl für Festkörperphysik, Universität Erlangen-Nürnberg, Staudtstrasse 7, D-91058 Erlangen, Germany*

Received 11 August 1994; accepted for publication 19 December 1994

**Abstract**

Basal plane surfaces of hexagonal silicon carbide samples of 6H and 4H polytype were investigated by means of low-energy electron diffraction (LEED). In a first part it is demonstrated by test calculations how diffraction spot intensities are dependent on the stacking sequence of the first few bilayers. It is shown that for an ideally flat sample it can be determined which specific layer of the hexagonal unit cell terminates the surface. However, when a statistical mixture of bilayer terminations is present on the surface, 4H and 6H polytypes yield indistinguishable intensities. In a second part a surface structure analysis based on experimental data obtained from two 6H-samples is presented. The surface orientation (polarity) is determined to be (0001) for both samples. Different termination morphologies are found which are clearly distinguishable by LEED. While one of the samples shows a mixed termination, the other exhibits a preferential termination with linear stacking of the first three bilayers involving typical step heights of three bilayer spacings or multiples of that. For this sample a refinement of the structure analysis shows that surface dangling bonds are saturated by hydroxyl species. Oxygen is found to be in atop position with a Si–O bond length of 1.65 Å. The asymmetric bond environment of the topmost Si leads to a contraction of the first bilayer (7.5%). The subsurface geometry is bulk-like.

*Keywords:* Low-energy electron diffraction (LEED); Silicon carbide; Surface structure

## 1. Introduction

Recent developments in the fabrication of electronic devices based on silicon carbide have triggered growing interest in the structural and electronic properties of this material. Based on its large band gap, temperature stability, thermal conductivity, high recombination rates and other properties it is now possible to manufacture a variety of unique devices including blue light emitting diodes, fast high power switches and more. A survey of electronic properties and technological applications was published recently [1].

A particularly interesting aspect of the crystal structure of SiC is the presence of a variety of allotropes, so called polytypes [2]. About 170 different polytypes of SiC have been identified experimentally so far [1]. Basic structural element of all SiC polytypes are hexagonal bilayers of alternating silicon and carbon atoms in tetragonal coordination similar to the structure of diamond or crystalline silicon (cf. Fig. 1a). The orientation and stacking sequence of bilayers determine the nature of the polytype. The probably most common structure is $\beta$-SiC, a modification in zincblende structure. All bilayers have the same orientation, i.e. the stacking

* Corresponding author. Fax: +49 9131 858400; E-mail: ustarke@erympel.rrze.uni-erlangen.de.


*SSDI* 0039-6028(95)00621-4

vector between each bilayer is pointing into the same direction, cf. Fig. 1b. Zincblende SiC is also called 3C-SiC indicating its cubic structure (C) with a hexagonal unit cell of 3 bilayer length along the [0001]-direction. $\alpha$-SiC polytypes contain bilayers in mutually different orientation resulting in hexagonal (H) or rhomboedric (R) structures. The simplest polytype of this kind, 2H-SiC, has wurtzite structure. Every second bilayer is rotated by 60° (or 180°) with respect to its neighbors. The corresponding hexagonal unit cell contains 2 bilayers. The stacking vector between bilayers is mutually pointing right and left in a $(11\bar{2}0)$-plane projection (cf. Fig. 1c). Polytypes 4H and 6H have a similar zig-zag stacking sequence. However, the stacking switch occurs after 2 and 3 bilayers, respectively, corresponding to hexagonal unit cells of 4 and 6 bilayer length, respectively (cf. Figs. 1d, 1e). All other modifications exhibit higher complexity (in the simplest rhomboedric polytype, 15R, the unit cell is repeated after 15 bilayers in

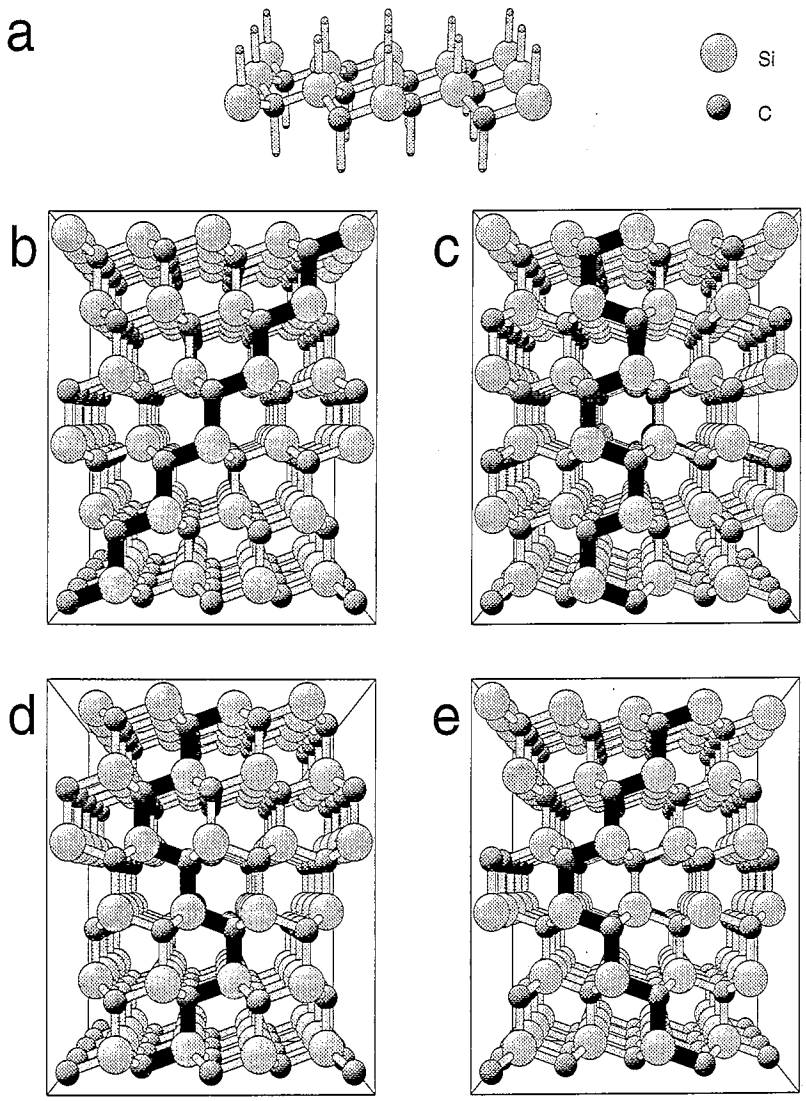


Fig. 1. Crystal structure of silicon carbide, side view along $(11\bar{2}0)$-direction: (a) hexagonal bilayer, (b) zincblende structure, 3C-SiC, (c) wurtzite structure, 2H-SiC, (d) 4H-SiC and (e) 6H-SiC. The stacking direction is depicted by the enhanced Si–C bond train parallel to the $(11\bar{2}0)$-direction.

[0001]-direction), and are not of interest in the present context.

Despite identical stoichiometry different polytypes have differences in their electronic gap energies of up to 1 eV (e.g. 2.39 eV for 3C-SiC, 3.33 eV for 2H-SiC, 3.02 eV for 4H-SiC [3]). This opens up interesting perspectives for the development of semiconductor sandwich devices, when epitaxial layers of different electronic properties can be grown without lattice mismatch. Even for electronic device production based on SiC in general, epitaxial layer growth is a necessary technique because the crystallin and electronic quality of bulk grown material is not sufficient. Unfortunately, the growth process of SiC layers of predesigned polytypes cannot yet be controlled with sufficient success [1]. It is possible to grow epilayers of a desired polytype using vicinal surfaces of a substrate of the same polytype [4]. However, on plane hexagonal surfaces of any polytype $\beta$-SiC is preferentially grown. Consequently, the structure and morphology of the hexagonal SiC-surface, which is the natural growth plane are relevant for some insight to the specific growth conditions necessary to obtain a specific polytype, and this interest has triggered the present work.

Surface studies and low-energy electron diffraction (LEED) investigations in particular of ordered SiC surfaces have been carried out earlier by a number of different groups [5–27]. However, only the (100)-surface of $\beta$-SiC has been analyzed quantitatively with respect to atomic geometries by LEED [15,16]. In all studies on hexagonal SiC-surfaces ordered structures were only reported after an extended heat treatment [5–11], combined with deposition of atomic silicon in some cases [12–14] to avoid the drawback of stoichiometric modifications due to different vapor pressures of silicon and carbon. Detailed atomic structures were not reported due to the lack of surface crystallographic methods.

In this paper we report about a detailed determination of the surface geometry of as grown hexagonal $\alpha$-SiC samples of 6H polytype. The work was concentrated on (0001)-surfaces which were investigated in ultrahigh vacuum (UHV) immediately after ex situ chemical preparation. We used LEED and Auger electron spectroscopy (AES) to analyze the composition and geometry of surfaces of epitaxial layer samples that were prepared by an oxidation and etching treatment without any heat treatment in UHV. Dynamical electron scattering calculations were applied to reproduce the experimentally obtained LEED intensities versus energy spectra ($I(E)$-spectra) from different samples. In addition to the structural analysis we present a theoretical investigation of the expected differences in the LEED data obtained from different polytypes (4H and 6H) and different surface terminations. The organization of the paper is as follows: after the present introduction we briefly describe the experimental procedures to obtain ordered surfaces in the next section. Section 3 is dedicated to a comparison of calculated intensity spectra obtained from different polytype and surface termination models. The actual geometry analyses are presented in Section 4 followed by a discussion and conclusion.

## 2. Samples

The experiments were carried out on epitaxial films grown by chemical vapor deposition on Lely-substrates and subsequently mechanically polished with a grain size as low as 0.25 $\mu$m [28]. The presence of a homogeneous polytype in the film was controlled by low-temperature photoluminenscence by the growers [28]. For the present study a chemical preparation procedure was applied to obtain flat and ordered surfaces as described in detail elsewhere [29]. Just briefly, the samples were oxidized at 800°C in 1 bar oxygen for about 4 hours. Contaminations were subsequently removed by acetone and aqua regia. The oxide layer on the SiC substrate was removed in hydrofluoric acid (50%) or buffered $NH_4F$ (pH 8.7). After a rinsing and drying treatment the samples were introduced into vacuum by a transfer mechanism. Without any further treatment a sharp $(1 \times 1)$ LEED pattern could be observed indicating a well-ordered surface with its unit cell corresponding to the SiC lattice. Note that ordered SiC surfaces cannot be obtained by means of in situ preparation alone (sputter/anneal cycles or silicon deposition) without a previous ex situ oxidation and etching treatment [29]. In normal electron incidence geometry $I(E)$-spectra of 3 symmetry inequivalent diffraction beams were acquired using an automated computer-controlled video LEED system (AutoLEED

[30,31]). A video recorder was used to reduce the necessary measurement time in order to avoid electron beam related intensity losses [29,32]. We used several different samples to control the reproducibility of the preparation treatment.

## 3. Model calculations for different polytypes and surface terminations

Full dynamical LEED calculations using standard computer programs [33] were carried out to generate $I(E)$ spectra based on theoretical models. Relativistically calculated and spin-averaged phase shifts were used based on potentials obtained from a 3C-SiC bulk crystal. From test calculations it was found that 11 phase shifts are sufficient for electron energies up to 500 eV while at least 13 phase shifts are necessary for energies up to 800 eV. Of course, with higher energies the electron can penetrate deeper into the surface where different polytypes should become distinguishable because of the different layer stacking. Aiming to avoid the large computer time required for 13 phase shifts we tested whether the high-energy range provides additional and unambiguous information about deeper layers using different values for the penetration depth. As that turned out not to be the case even for relatively low attenuation the energy was restricted to a maximum of 500 eV throughout the structure analysis. Technically, the electron attenuation was simulated by the imaginary part of the optical potential $V_{0i}$. The damping term was considered energy dependent: $V_{0i} \sim E^{1/3}$. In this paper the actual values of $V_{0i}$ at 90 eV are given rather than the proportionality factor. Layer diffraction matrices were calculated by Beeby's matrix inversion scheme [34]. Individual bilayers (cf. Fig. 1a) had to be treated as composite layers using the combined space method [33,35] to account for the small vertical spacing of 0.63 Å within an individual bilayer. Scattering between bilayers was modeled using the layer doubling scheme [36,37]. In some cases, the first layer was considered to have a chemical composition different from the bulk stoichiometry. In the calculations this was modeled using the averaged $t$-matrix approximation (ATA) where the scattering amplitudes of two elements are averaged according to the atomic concentration [38–40]. Geometry (interlayer distances), composition, Debye temperatures, $V_{0i}$ as well as the real part of the inner potential $V_{0r}$ were included as parameters in the fit procedure. As usual in LEED structural determinations this comparison of experimental data and model calculations was carried out by $R$-factors [41,31]. Pendry's $R$-factor $R_p$ [42] is particularly useful for the present investigation because the chemically prepared samples are electron beam sensitive with a loss of order obviously induced in the near surface region [29]. Due to the energy-dependent penetration depth of the LEED electron this sensitivity causes the overall slope of the $I(E)$-spectra to change with the electron dose. Accordingly, the absolute intensities are not well defined in the experiment whereas the structural features are preserved in detail [29]. $R_p$ is ideal for this situation because it compares peak positions and peak shapes rather than absolute intensities. The limits of error were estimated by the variance of Pendry's $R$-factor $\mathrm{var}(R_p) = R_{min} \times \sqrt{8V_{0i}/\Delta E}$ [42] (where $\Delta E$ is the total energy overlap between experimental and calculated data). In all cases the size of the data base was sufficient for an unambiguous model selection. The corresponding limits of error on structural parameters can be deduced from $R$-factor plots.

In the context of epitaxial growth the structural analysis of hexagonal SiC-surfaces deals with two in principle different aspects: first, the determination of atomic geometries in the outermost layer(s) can provide information about the saturation of dangling bonds on clean surfaces and about chemisorption positions of C or Si atoms or related molecules. This might allow predictions for favorable parameters to achieve a certain stacking direction for the deposition of an additional layer. Second, the identification of the polytype of a surface region needed to control the result of the crystal growth requires sufficient sensitivity to registry parameters several layers below the surface, i.e. to the bilayer stacking sequence. The first aspect is straightforward for LEED crystallography. In the present analysis a variety of parameters including adatom positions is considered and a clear best-fit can be achieved as shown below. The second aspect introduces more difficulties for LEED due to the limited penetration depth of the electrons. In the present section a theoretical investigation of related problems is presented where calculated data

from different polytypes are compared. The long vertical unit cell length ($c$-length) of polytypes implies an additional complication when 4 or 6 different surface layer terminations have to be considered in 4H or 6H polytypes, respectively. Last but not least, these terminations may or may not be present as a mixture on the surface. In this context we have considered two extreme cases of possible surface geometries by comparing theoretical spectra from different individual termination structures. Also and in the same way we investigated samples of different polytype with a statistical mixture of terminations present on the surface.

In order to check for the influence of the surface termination on $I(E)$-spectra, a surface slab of $c$-length thickness was used, i.e. 4 and 6 bilayers for 4H and 6H samples, respectively. Layer distances were assumed to be bulk-like. In this model different surface terminations are equivalent to different bilayer stacking sequences. Three and two different slab models had to be calculated for the two polytypes, 4H and 6H, respectively, with other terminations symmetrically equivalent with respect to a mirror plane due to the hexagonal crystal structure. All spectra were averaged with respect to this mirror plane to account for the sixfold symmetry of the diffraction pattern. Fig. 2 shows the bilayer stacking in a projection on the $(11\bar{2}0)$-plane. The resulting $I(E)$-spectra are rather different for different surface terminations. However, different polytypes yield similar spectra when the stacking switch occurs in the same layer. This is clear from visual inspection of the spectra (cf. Fig. 3) as well as from $R_p$-factor analysis. For example the (10)-spectra from 4H and 6H calculated in normal incidence geometry compare as $R_p = 0.18$ with a 2nd layer switch (S2-4H, S2-6H, cf. Fig. 2) and as $R_p = 0.30$ with a 3rd layer switch (S3-4H, S3-6H) while comparison of structures with mutually different stacking yields $R_p = 0.65$ at best. Fig. 3a depicts the respective structural differences and similarities in the (10)-spectra. Only selected features allow for the discrimination between different terminations, e.g. the peak group between 100 eV and 150 eV while others are insensitive to stacking, e.g. the two peaks below 100 eV. Qualitatively similar results are obtained from calculations in off-normal incidence geometry with a tilt angle of 50° in $(11\bar{2}0)$-direction so that the incoming electrons penetrate almost parallel to the bilayer stacking vector. This geometry was chosen to enhance the sensitivity to the bilayer orientation. In Fig. 3b the (02) spectra are displayed, corroborating the sensitivity to the stacking sequence when the switch occurs in the 2nd or 3rd layer. However, it can also be seen that for the 6H sample BCACBA

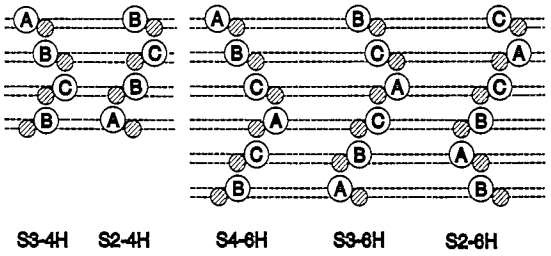


Fig. 2. Stacking termination structures possible in 6H and 4H polytypes displayed for one unit cell, corresponding to the slabs used in the calculations. Each slab is labeled according to the depth of the stacking switch and its polytype.

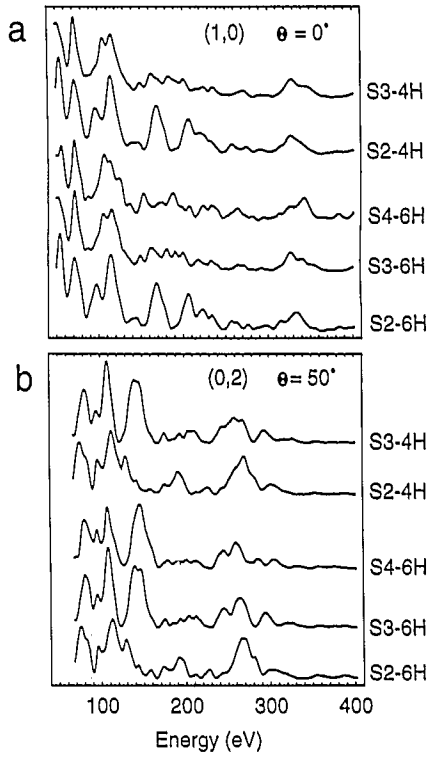


Fig. 3. Theoretical $I(E)$-spectra obtained from single termination models (slabs): (a) (10)-spectra in normal incidence condition, (b) (02)-spectra in off-normal incidence condition at 50° angle in $(11\bar{2}0)$-direction.

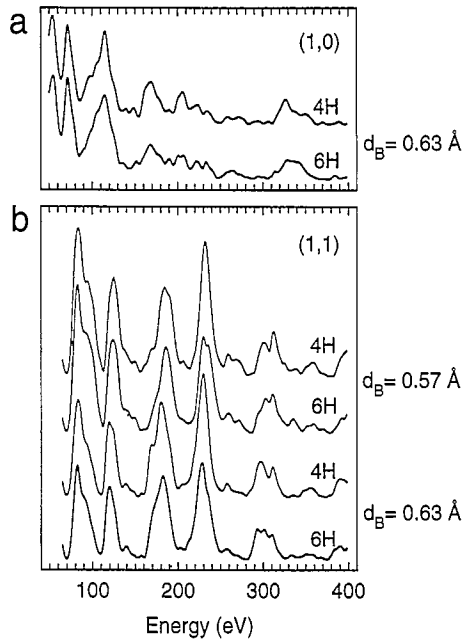


Fig. 4. Theoretical $I(E)$-spectra obtained from termination mixtures in normal incidence condition comparing 6H and 4H polytype samples: (a) (10)-spectra in bulk like geometry, (b) (11)-spectra with 0% and 10% contraction of the outermost bilayer.

and ABCACB (S3-6H, S4-6H, cf. Fig. 2) are hardly distinguishable due to the long electron path necessary to reach the stacking switch.

As a consequence of the results of the above slab calculations, a distinction of different polytypes (6H and 4H) with a mixed termination morphology is rather difficult. This is demonstrated in Fig. 4a for the (10)-spectra of 6H and 4H samples with equally weighted mixtures of possible terminations. The formerly well resolved and termination sensitive features of the 100–150 eV peak group are now smeared out and very similar for the two polytypes. For the (11)-spectra one observes slight differences between the 6H and 4H structures, e.g. at 180 eV and around 300 eV. However, the differences are of the same magnitude as a 10% variation of the first bilayer thickness would yield as depicted in Fig. 4b where 4H and 6H data are shown for $d_B = 0.63$ Å (bulk-like) and $d_B = 0.57$ Å, respectively. It should be noted that the above mixed structures were calculated using a full SiC bulk rather than the slab model discussed before. In test calculations it was verified that no significant differences in the spectra are caused by the different model.

## 4. Structure analysis

### 4.1. Experimental data

Several 6H-SiC(0001) samples were experimentally investigated [29]. Although for all samples the same preparation procedure was used, two distinguished surface conditions were found as reflected by their $I(E)$-spectra serving as fingerprint for the surface structure. Correspondingly, two different complete $I(E)$-data sets (sample 1,2) were included in the structure determination. In general, the two data sets are rather similar, especially at high energies. However, two main differences are conspicuous: first, the spectra of the second data set are much richer in structure. As the electron damping in the two samples is rather unlikely to be different, this fact indicates the presence of some disorder or of a mixture of different structures on sample 1. This compares to a single domain structure obviously present on the surface of sample 2. A second finding corroborates this interpretation, namely the appearance of a few distinct structural features in the spectra of sample 2 that are missing or at least blurred in data set 1. Both effects are displayed in Fig. 5 for the (11)-beam. The spectrum from sample 1 is much smoother than that from sample 2, and at 330 eV a peak present in curve 2 is missing in curve 1 as depicted by the hatched area.

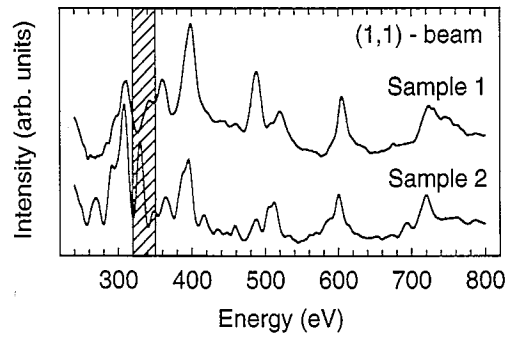


Fig. 5. Experimental (10)-spectra from two different typical samples (1,2). A significant difference is depicted by the hatched area.

### 4.2. Model variations

In a first step the two data sets were fitted by model calculations for clean SiC, i.e. we neglect the saturation of dangling bonds by impurities. Adatoms were introduced in a refinement fit as second step. The clear $R$-factor minimum for the final substrate model as well as the improvement by introducing adatoms justify this approach, as will be demonstrated in the following sections. In the substrate analysis step the topmost bilayer could be considered complete because a half bilayer termination is equal to a bond saturating carbon adatom and was correspondingly included in step two for practical reasons. In the structural search the bilayer height $d_B$ was varied from 0.50 to 0.75 Å around the bulk value of 0.63 Å. Additionally, the first three inter-(bi-)layer spacings ($d_{12}$, $d_{23}$, $d_{34}$) were varied, too (1.89 Å ± 3%). In some cases the variation range was expanded until a minimum was found. It should be noted that the variation of $d_B$ is much more expensive in terms of computer time because a composite layer must be recalculated while for different spacings between bilayers only a different stacking parameter is used for layer doubling. Accordingly, we restricted the variation of $d_B$ to the first bilayer. Any non-bulk-like bilayers deeper in the surface would thus corrupt the interlayer spacing result. However, the center of mass plane of the bilayer should come out fairly accurate as also found for buckling features in many LEED investigations.

The surface orientation (polarity) of the epitaxial film samples was nominally (0001), i.e. silicon-terminated as suggested by the substrate orientation [28]. However, because this was not checked by crystallographic methods, the polarity was included as an additional fit parameter. Non-bulk-like stoichiometry was allowed on the surface by considering up to 100% carbon enrichment in the topmost bilayer. For both samples each single stacking termination was calculated and fitted separately. In addition, several different mixtures of terminations were included. As outlined before, three different stacking terminations have to be calculated for a 6H structure. All mixtures were considered as incoherent mixtures and simulated by intensity averaging. It should be noted, however, that a full structural variation combined with a percentage variation of structural mixtures goes beyond any computational capacity. So, only a selection of reasonable mixtures could be investigated (see below). In addition to the bulk-like stacking models a 2H stacking on the surface (ABABC...) was taken into account.

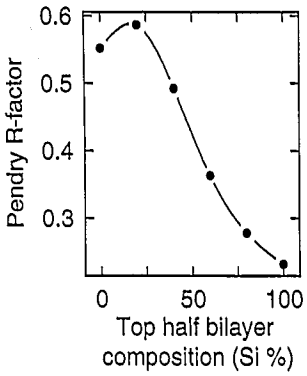


Fig. 6. $R$-factor plot for a variation of the Si content in the top-half bilayer.

### 4.3. Substrate structure

The surface polarity was determined in a first step using a coarse grid for the variation of geometry parameters. Individual stacking terminations as well as equally weighted mixtures were compared to the experiment. In this case only structures with identical geometries were mixed in order to save computer time. Additionally, a variation towards carbon rich composition was allowed for the first bilayer using ATA as outlined before. Fig. 6 shows the respective $R$-factor plot (for the best-fit geometry, see below) of sample 1 depicting a clear minimum for 100% Si content of the top half bilayer, i.e. bulk-like stoichiometry. For both samples $(000\bar{1})$-orientation (carbon side) could be excluded ($R_p \geq 0.65$) for any termination model. A much better fit was achieved for the expected (0001)-orientation for both samples. However, different termination morphologies are preferred by the structural fit. For sample 1 with the smoothly structured $I(E)$-spectra a mixture of all possible terminations yields $R_p = 0.23$, significantly better than individual terminations (0.44, 0.35 and 0.49 for ABCACB, BCACBA and CACBAB, respectively). For sample 2 a single termination, namely ABCACB is preferred with $R_p = 0.33$ as compared to 0.52 and 0.55 for the other terminations

and 0.39 for a mixed structure. In Fig. 7 the best-fit spectra (dashed lines) are displayed for the (10)- and (20)-spot. Additionally, for the (11)-spot the best-fit spectra for all single terminations and the mixed structure are compared with the experimental data. In this panel it can be seen to what extent the experimental data different for the two samples (cf. Fig. 5) can be reproduced by the best-fit models. In summary, the substrate analysis step finds the two experimental structures distinguished by their termination morphology. Sample 1 is composed of all possible 6H-stacking terminations while on sample 2 only the ABCACB stacking is present on the surface. Table 1 displays the complete geometry of both structures. It should be noted that with none of the "clean" surface full bilayer models the low-energy range (below 250 eV) was well reproduced in the calculations, obviously due to an incorrect description of the immediate surface region. In the substrate analysis step this was accounted for by cutting the low-energy data below around 250 eV. In order to account for low-intensity measurement problems the spectrum of the (11)-beam was cut off below 290 eV for sample 1.

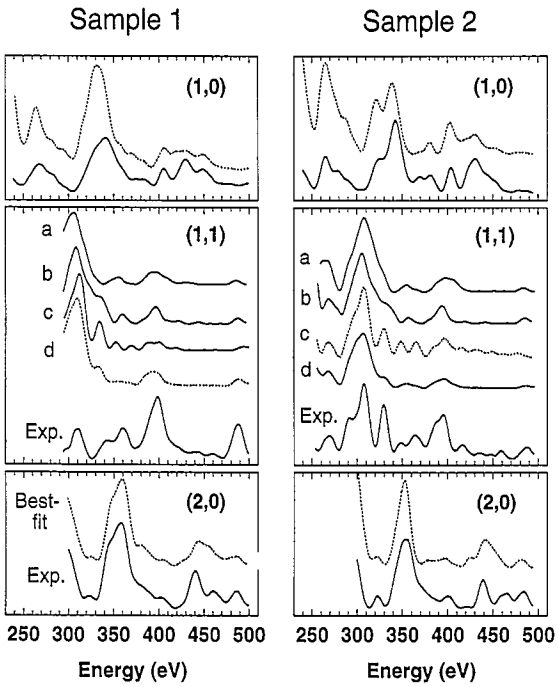


Fig. 7. Best-fit spectra for sample 1 (left) and 2 (right) in a "clean" surface full-bilayer model ((10)-, (11)- and (20)-beams, normal incidence). Experimental data (bottom of each panel) are compared to the best-fit (dashed line) and for the (11)-beam to spectra obtained for CACBAB indicated as (a), BCACBA (b), ABCACB (c) and mixed termination (d) models. $R_p = 0.23$ (sample 1), $R_p = 0.33$ (sample 2).

Table 1
Best-fit results for sample 1 and 2 in the "clean" surface model and sample 2 in the T1-oxygen model

| | Sample 1 Mixed terminations "clean" surface | Sample 2 ABCACB "clean" surface | Sample 2 ABCACB T1-oxygen |
|---|---|---|---|
| $d_{01}$ (Å) | – | – | 1.65(3) |
| $d_B$ (Å) | 0.65(3) | 0.52(5) | 0.58(3) |
| $d_{12}$ (Å) | 1.83(3) | 1.92(4) | 1.90(2) |
| $d_{23}$ (Å) | 1.95(3) | 1.88(4) | 1.89(2) |
| $d_{34}$ (Å) | 1.89(3) | 1.92(4) | 1.88(3) |
| $V_{0r}$ (eV) | −7.0(2.0) | −13.5(2.0) | −13.0(1.5) |
| $V_{0i}$ (eV) | −4.0 | −4.0 | −3.5 |
| $R_p$ | 0.23 | 0.33 | 0.23 |

### 4.4. Dangling bond saturation

Adatom models were introduced for sample 2 in the single termination model found in the substrate analysis step. This sample was chosen in order to avoid possible complications of the adatom variation with the mixing ratio. For sample 1 a reasonably safe analysis including both issues probably would require a larger experimental data base. Carbon and oxygen were chosen as possible adatoms, representing a half bilayer model (carbon) or a saturation of dangling bonds with hydroxyl species (neglecting hydrogen in the calculation) as suggested by vibration spectroscopy [29,32]. Three different high-symmetry sites were tested as illustrated in Fig. 8. T1 represents the atop site, T4 the three-fold hollow site with a fourth atom (carbon) closely coordinated in the top bilayer, and H3 the remaining three-fold hollow site with no further neighboring atom. For all sites the adatom height was varied in addition to the layer spacings described before. A clear best-fit was achieved for oxygen termination in the T1 site with $R_p = 0.23$, while T1-carbon yields $R_p = 0.40$, and other sites 0.47 at best (compare $R_p = 0.33$ for the substrate model best-fit). In this analysis step the low-energy data were included and well reproduced

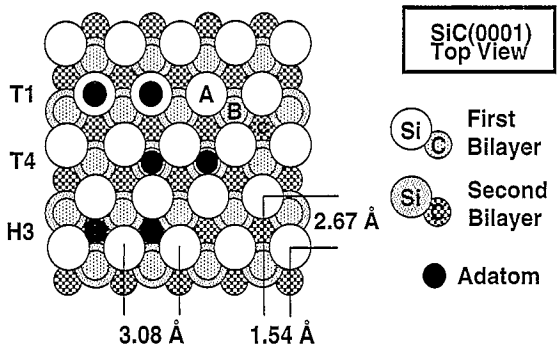


Fig. 8. Adatom (or molecular) site models on a (0001)-SiC surface: T1: atop site; T4: 3-fold site with an additional neighbor in the low-half top bilayer; H3: 3-fold site without additional coordination.

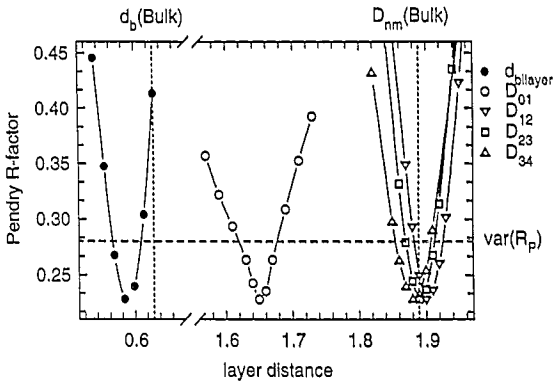


Fig. 10. $R$-factor plot for oxygen bond length, topmost bilayer thickness and interlayer spacings in the T1-oxygen model (sample 2).

as elucidated in Fig. 9. Due to the convergence limit of layer doubling, adatom to topmost silicon spacings $d_{01} < 1.0$ Å were not tried. For the T1 and T4 sites this seems justified considering hard core radii. Only for the H3 site lower adatom positions are feasible in that respect. However, such a high coordination of oxygen in a covalent crystal environment would hardly be understandable from a chemical point of view. Correspondingly, this was not included in the analysis in order to avoid the then necessary very expensive composite layer calculation, also because no tendency for better $R$-factors was found lowering $d_{01}$ down to 1.0 Å. In the best-fit model the silicon–oxygen bond length is $d_{01} = 1.65$ Å. The outermost bilayer is slightly contracted (7.5%) to $d_B = 0.58$ Å due to the asymmetric bond coordination of the topmost silicon. In contrast to the "clean" surface best-fit models (cf. Table 1) here the interbilayer spacings are at bulk value within the error margin. The complete geometry is included in Table 1 as well. Fig. 10 shows $R$-factor plots for all layer distances including the var($R_p$) level used for the error assessment. To further justify the approach of separating substrate model and adatom fit an oxygen adatom model was tested on the BCACBA substrate termination yielding no $R$-factor improvement at all ($R_{p,min} = 0.53$).

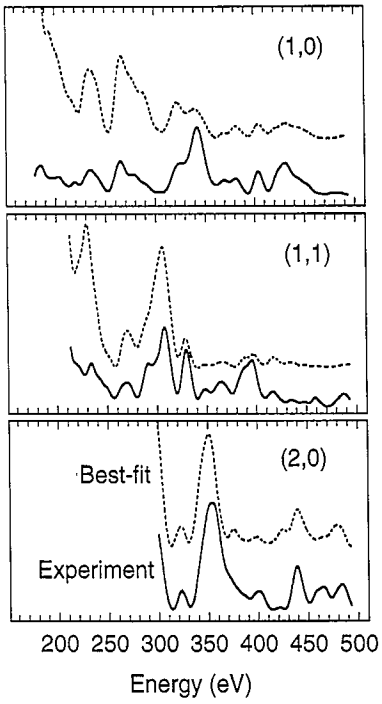


Fig. 9. Best-fit spectra for sample 2 in single ABCACB termination with oxygen in a T1-site at a Si–O bond length of 1.64 Å, $R_p = 0.23$.

## 5. Discussion

The surface structures obtained for two samples of 6H-SiC(0001) in this investigation are considerably different from each other. One shows a mixture of different surface terminations while the other has a rather pure structure with only one termination present where the three outermost bilayers are linearly stacked representing the maximum possible for

6H. The reason for the difference may be caused by not yet sufficiently controlled parameters in the preparation procedure but this requires further experimental investigation. In addition, for sample 2 a saturation of the surface dangling bonds with oxygen in atop positions (T1-site) could be determined. Unexpectedly, the distinction of carbon and oxygen in this position was very clear despite the rather similar scattering properties. Both features of sample 2, the oxygen adatoms and the single termination morphology are in agreement with other experimental observations [29]: in LEED some electron beam sensitivity was found which was interpreted to be due to hydroxyl groups residual on the surface after the chemical preparation treatment as identified by vibration spectroscopy and AES [29,32]. For two different 6H-samples scanning tunneling microscopy (STM) found a step morphology where step heights are multiples of three bilayer spacings, so corroborating a single termination model [29,43]. This termination is found to be ABCACB by the present study.

Comparison of calculated spectra showed that samples with single terminations are clearly distinguishable, whilst polytypes with mixed structures are not. However, as the present structure analysis and STM work shows, the terminations are not necessarily present in a statistical mixture, at least under certain conditions. Provided the observed ABCACB stacking structure found indicates a trend for linear stacking maintained as far as possible on the surface, a distinction of polytypes should be possible to the same extent as the individual terminations are distinguishable. In case of linear stacking being indeed energetically favorable on the surface we might have found a reason why on flat surfaces exactly this linear stacking is preferred during growth (leading to 3C films) unless the (probably small) energy difference is compensated by the defect energy of lateral domain boundaries when the structure actually is conditioned to hexagonal stacking e.g. due to a surface miscut.

## Acknowledgements

This work was supported by Deutsche Forschungsgemeinschaft (DFG) through Sonderforschungsbereich 292. U.S. is grateful to DFG for additional financial support. The authors are indebted to Professor Dr. R. Helbig for providing the SiC samples.

## References

[1] G. Pensl and R. Helbig, Silicon carbide (SiC) – recent results in physics and in technology, in: Festkörperprobleme/Advances in Solid State Physics, Vol. 30, Ed. U. Rössler (Vieweg, Braunschweig, 1990) p. 133.
[2] R. Verma and P. Krishna, Polymorphism and Polytypism in Crystals (Wiley, New York, 1966).
[3] W.J. Choyke, Optical and electronic properties of SiC, in: The Physics and Chemistry of Carbides, Nitrides and Borides, Ed. R. Freer (NATO ASI Series, Manchester, 1989).
[4] H. Matsunami, K. Shibahara, N. Duroda, W. Yoo and S. Nishino, VPE growth of SiC on step-controlled substrates, in: Amorphous and Crystalline Silicon Carbide and Related Materials, Eds. G.L. Harris and C.Y-W. Yang (Springer, Berlin, 1989) p. 34.
[5] A.J. van Bommel, J.E. Crombeen and A. van Tooren, Surf. Sci. 48 (1975) 463.
[6] F. Bozso, L. Muehlhoff, M. Trenary, W.J. Choyke and J.T. Yates Jr., J. Vac. Sci. Technol. A 2 (1984) 1271.
[7] C-S. Chang, I.S.T. Tsong, Y.C. Wang and R.F. Davis, Surf. Sci. 256 (1991) 354.
[8] L. Muehlhoff, M.J. Bozack, W.J. Choyke and J.T. Yates, J. Appl. Phys. 60 (1986) 2558.
[9] L. Muehlhoff, W.J. Choyke, M.J. Bozack and J.T. Yates, J. Appl. Phys. 60 (1986) 2842.
[10] S. Nakanishi, H. Tokutaka, S. Nishimori, S. Kishida and N. Ishihara, Appl. Surf. Sci. 41/42 (1989) 44.
[11] P. Heuell, M.A. Kulakov, V.F. Tsvetkov and B. Bullemer, in: Silicon Carbide and Related Materials, Eds. M.G. Spencer et al. (Institute of Physics, Bristol, 1995) p. 365.
[12] R. Kaplan and T.M. Parrill, Surf. Sci. 165 (1986) L45.
[13] R. Kaplan, J. Vac. Sci. Technol. A 6 (1988) 829.
[14] R. Kaplan, Surf. Sci. 215 (1989) 111.
[15] J.M. Powers, A. Wander, P.J. Rous, M.A. Van Hove and G.A. Somorjai, Phys. Rev. B 44 (1991) 11159.
[16] J.M. Powers, A. Wander, M.A. Van Hove and G.A. Somorjai, Surf. Sci. 260 (1992) L7.
[17] S. Adachi, M. Mohri and T. Yamashina, Surf. Sci. 161 (1985) 479.
[18] J.J. Bellina, Jr. and M.V. Zeller, Appl. Surf. Sci. 25 (1986) 380.
[19] V.M. Bermudez, J. Appl. Phys. 66 (1989) 6084.
[20] V.M. Bermudez, Surf. Sci. 276 (1992) 59.
[21] M. Dayan, J. Vac. Sci. Technol. A 4 (1986) 38.
[22] J.A. Dillon, Jr., R.E. Schlier and H.E. Farnsworth, J. Appl. Phys. 30 (1959) 675.
[23] J.T. Grant and T.W. Haas, Phys. Lett. 33 A (1970) 386.
[24] S. Hara, W.F.J. Slijkerman, J.F. van der Veen, I. Ohdomari, S. Misawa, E. Sakuma and S. Yoshida, Surf. Sci. 231 (1990) L196.

[25] B. Jorgensen and P. Morgen, J. Vac. Sci. Technol. A 4 (1986) 1701.
[26] T.M. Parrill and Y.W. Chung, Surf. Sci. 243 (1991) 96.
[27] J.M. Powers and G.A. Somorjai, Surf. Sci. 244 (1991) 39.
[28] S. Karmann, W. Suttrop, A. Schöner, M. Schadt, C. Haberstroh, F. Engelbrecht, R. Helbig and G. Pensl, J. Appl. Phys. 72 (1992) 5437.
[29] U. Starke, C. Bram, P.-R. Steiner, W. Hartner, L. Hammer, K. Heinz and K. Müller, Appl. Surf. Sci. 89 (1995) 175.
[30] K. Müller and K. Heinz, Computer-controlled LEED intensity and spot profile determination, in: The Structure of Surfaces, Eds. M.A. Van Hove and S.Y. Tong (Springer, Berlin, 1985) p. 105.
[31] K. Heinz, Prog. Surf. Sci. 27 (1988) 239.
[32] P.-R. Steiner, L. Hammer, U. Starke and K. Müller, in preparation.
[33] M.A. Van Hove and S.Y. Tong, Surface Crystallography by LEED (Springer, Berlin, 1979).
[34] J.L. Beeby, J. Phys. C 1 (1968) 82.
[35] S.Y. Tong and M.A. Van Hove, Phys. Rev. B 16 (1977) 1459.
[36] J.B. Pendry, Low Energy Electron Diffraction (Academic Press, London, 1974).
[37] M.A. Van Hove and J.B. Pendry, J. Phys. C 8 (1975) 1362.
[38] Y. Gauthier, Y. Joly, R. Baudoing and J. Rundgren, Phys. Rev. B 31 (1985) 6216.
[39] Y. Gauthier and R. Baudoing, in: Low Energy Electron Diffraction from Alloy Surfaces, Eds. P. Dawben and A. Miller (CRC Press, Boca Raton, FL, 1990) p. 169.
[40] S. Crampin and P.J. Rous, Surf. Sci. 244 (1991) L137.
[41] M.A. Van Hove, W.H. Weinberg and C.M. Chan, Low Energy Electron Diffraction, Vol. 6 of Springer Series in Surface Science (Springer, Berlin, 1986).
[42] J.B. Pendry, J. Phys. C 13 (1980) 937.
[43] U. Starke, J. Schardt, C. Bram, P.R. Steiner, W. Hartner, S. Müller, L. Hammer, K. Heinz and K. Müller, in: Proc. Symp. Surf. Sci. 3S'95, Eds. P. Varga and F. Aumayr, Kitzsteinhorn (1995) p. 11.